Correlation between laser-induced damage densities of fused silica and average incubation fluences at 1064nm in the nanosecond regime

Laurent Lamaignère, Romain Diaz, Maxime Chambonneau, Pierre Grua, Jean-Yves Natoli, Jean-Luc Rullier

Correlation between laser-induced damage densities of fused silica and average incubation fluences at 1064 nm in the nanosecond regime

L. Lamaignère, R. Diaz, M. Chambonneau, P. Grua, J.-Y. Natoli, and J.-L. Rullier

Citation: J. Appl. Phys. **121**, 045306 (2017); doi: 10.1063/1.4974945
View online: http://dx.doi.org/10.1063/1.4974945
View Table of Contents: http://aip.scitation.org/toc/jap/121/4
Published by the American Institute of Physics

Correlation between laser-induced damage densities of fused silica and average incubation fluences at 1064 nm in the nanosecond regime

L. Lamaignère,[1,a)] R. Diaz,[1] M. Chambonneau,[1] P. Grua,[1] J.-Y. Natoli,[2] and J.-L. Rullier[1]
[1]*CEA, CESTA, F-33116 Le Barp, France*
[2]*Aix Marseille Université, CNRS, Centrale Marseille, Institut Fresnel, UMR 7249, 13013 Marseille, France*

(Received 10 October 2016; accepted 13 January 2017; published online 26 January 2017)

The chronology of the physical processes involved in the nanosecond laser damage of fused silica is investigated at 1064 nm. From experiments realized with multiple longitudinal mode pulses, the correspondence between ring pattern damage morphology and the corresponding intensity profile allows the distinction of two damage phases: an incubation phase followed by a damage expansion phase that leads to the final damage diameter. It allows us to determine both the incubation and the expansion fluences. These results are compared to damage density measurements for different laser configurations, different optics, and different environments. It was found that damage densities were as high as incubation fluences were low. This approach shows a deterministic part of laser damage in nanosecond regime and contributes to reinforce the statistical results by reducing their random nature and is more able to guide the physical interpretations of laser damage experiments. *Published by AIP Publishing*. [http://dx.doi.org/10.1063/1.4974945]

I. INTRODUCTION

The reported work makes the link between the probabilistic nature of the rear surface laser damage at 1064 nm in the nanosecond regime and a deterministic aspect characterized by a linear relation between damage diameters and expansion fluence. Up to now, the probabilistic aspect is dealt with statistical analysis and the laser-induced damage (LID) density is the main measurand describing a damage distribution. In most cases, damage density is obtained by means of 1-on-1[1] procedure that measures high damage densities[2,3] and/or rasterscan procedure that measures low ones.[4,5] These two procedures are complementary and permit us to compare the damage resistance of several optical components. This statistical study is useful when considering the effects of beam and pulse parameters leading to a qualitative comparison without physical interpretation. It has been recently shown that damage diameter, in the case of ring pattern damage due to multiple longitudinal modes (MLMs) pulses, makes possible the estimation of the expansion fluence leading to the final damage size: this result highlights a deterministic behavior of the damage in the nanosecond regime.[6,7] From damage diameter measurements, it is easier to analyze a part or even the whole statistical results for given experiments: damage densities (ρ) and damage diameters (dd) are correlated.

In this paper, we compare two different experiments realized on fused silica samples at 1064 nm in the nanosecond range using a Nd:YAG laser source working in the MLM regime. In these experiments, the laser beam is collinear through the sample thickness and then, damage sites were observed only at the exit surface of fused silica. The first experiment consists in a single laser irradiation of a site in order to correlate precisely the damage morphology and the corresponding intensity temporal profile. Actually, MLM pulses provide a powerful tool that allows us to investigate the chronology of the physical processes involved in laser induced damage by dividing the damage initiation in two phases. The first one corresponds to the incubation of the damage precursor; the second phase corresponds to the expansion of the damaged area. For the second phase, it is possible to establish an accurate relation between the final damage diameter and the corresponding expansion fluence. This experiment has been repeated several times in order to scan a wide range of fluences. For a given laser configuration, damage diameters have been precisely measured, and incubation as well as expansion fluences have been accurately determined with the procedure described in Ref. 6: these data give access to the deterministic part of the laser induced damage mechanisms. This aspect has been studied by Papernov and Schmid on artificial defects embedded in SiO_2 thin films.[8] The second experiment consists in the determination of the damage density, many sites being irradiated: this experiment leads to quantify the well-known statistical behavior of the laser-optics interaction.[2,5,9,10] The two sets of experiments are compared, and the statistical results are analysed with the help of the deterministic ones. We highlight that damage densities can be correlated to incubation fluences. Such comparison is realized for several laser configurations and several optical components. It is then shown that it is possible to make a better analysis of damage densities results from the estimation of the incubation fluence. In Section II of this paper, the physical phenomenon that permits us to match up damage morphologies and intensity profiles is presented. Section III is devoted to the methodology developed for the comparison of the damage densities with the deterministic approach. It is implemented for a specific configuration: the impact of the environment (air and vacuum) on laser damage. On this basis, different configurations are studied in Section IV, including the

[a)]laurent.lamaignere@cea.fr

change in laser polarization, the modification of surface roughness and the choice of laser mode composition. Finally, the comparison between deterministic and statistical results is discussed in Section V.

II. HIGHLIGHTS OF TWO REGIMES IN THE INITIATION PROCESS

An original experiment performed with multiple longitudinal modes (MLMs) pulses had permitted us to investigate the ring pattern formation occurring during the laser-induced damage (LID) at 1064 nm, leading to an in-depth analysis of the damage initiation processes. As described in Refs. 6 and 11, the temporal profile of the pulse can be matched with the damage ring pattern. Each intensity spike is accurately associated with a unique ring as shown in Figure 1 for a damage site initiated at 110 J/cm^2. Then, the time t_0, associated with the starting of an activation front on the optics surface is determined,[6] and two damage formation phases are distinguished. The first one corresponds to the absorption of the laser flux by a subsurface defect (a damage precursor like a subsurface fracture) until t_0. During this phase, the deposited energy will induce silica vaporization in the crack and generate a pressure field, which may be able to widen and propagate the fracture up to the silica surface, leading to the ejection of a plasma,[12,13] this making the surrounding surface absorbent.

The second phase, starting at t_0, is related to the damage expansion up to the end of the pulse: the removal of material is due to an ablation process subsequent to the activation of the silica surface provided by the diffusive expansion of the plasma at the vicinity of the surface.[14] Thus, one can separate the total fluence experimentally measured as[6]

$$F_{tot} = F_{inc} + F_{exp}; \quad F_{inc} = \int_{-\infty}^{t_0} I(t')dt'; \quad F_{exp} \int_{t_0}^{+\infty} I(t')dt', \tag{1}$$

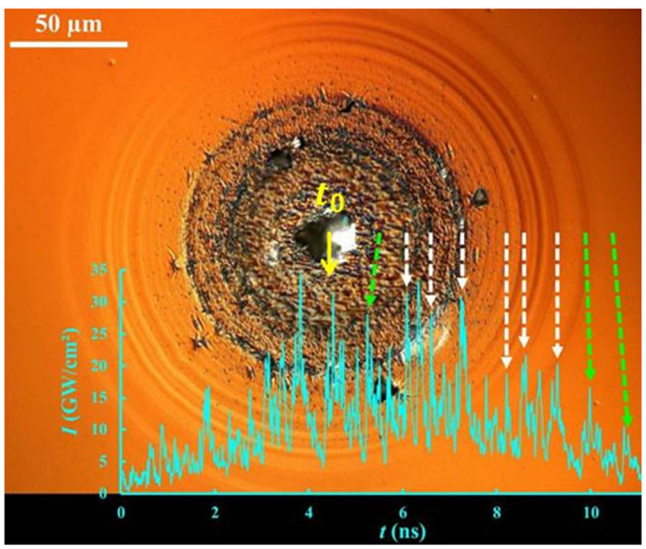

FIG. 1. Correlation between the morphology of a damage site, initiated at 1064 nm and 110 J/cm^2 on the rear surface of a fused silica sample, and the corresponding MLM pulse temporal profile.

where F_{inc} and F_{exp} relate to the incubation by the precursor defect and the expansion of the ring pattern, respectively. With the approximation that $I(t) \approx I_{avg}$, then Equation (1) becomes

$$F_{tot} \approx \tau \cdot I_{avg} \approx \tau_{inc} I_{avg} + \tau_{exp} I_{avg}, \tag{2}$$

where τ is the pulse duration, τ_{inc} refers to the incubation duration of a precursor defect up to t_0 and τ_{exp} stands for the expansion duration. During this second phase, the plasma expansion leads to the ring pattern formation with a ring appearance speed given by $v = aI_{avg}{}^b$, where a and b are equal to 9.3 km cm^{2b} GW^{-b} s^{-1} and 1/3 in air environment, respectively.[7] Then, for a given F_{tot}, the apparent diameter Φ of the damage site at the end of the pulse can be written as

$$\Phi = 2v\tau_{exp} = 2a\left(\frac{\tau}{F_{tot}}\right)^{1-b} F_{exp}. \tag{3}$$

As a consequence, at a given F_{tot} the outer diameters are directly proportional to the expansion fluence and the coefficient of Equation (3) is directly given by the experimental conditions which are: the laser pulse duration (τ), the fluence of the pulse (F_{tot}), and the two parameters describing the ring appearance speed v (a and b).

An example of such analysis is shown in Fig. 2, for irradiations of several sites at fluences ranging from 75 to 120 J/cm^2 and a total pulse duration close to 10 ns (the full width at half maximum (FWHM) for the equivalent Gaussian temporal profile is 6.5 ns). For each damage site, the expansion fluence F_{exp} (blue arrow) is determined integrating the intensity (I) over time after t_0 to the end of the pulse; the incubation fluence F_{inc} (green arrow) is deduced making the difference between F_{tot} and F_{exp} (this fluence can also be determined integrating the intensity (I) over time up to t_0). Equation (3), with $F_{tot} = 100$ J/cm^2 represented by the dashed line linearly correlates damage diameters with expansion fluences only (dd with F_{exp}).

Incubation fluences (represented by the green arrows) are dispersed. They vary from 30 to 80 J/cm^2 for experiments realized around 100 J/cm^2, this dispersion is supposed to arise from the randomness of the precursor characteristics

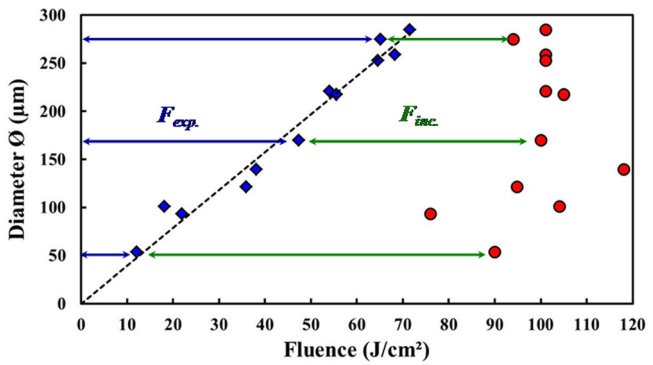

FIG. 2. Damage diameter as a function of the total fluence (red circles) and the damage expansion fluence (blue squares). The green arrows indicate for 3 damage sites the incubation fluence which is the difference between total fluence and expansion fluence. The linear behavior (black dashed line) obtained with Eq. (3) corresponds to $a = 9.3$ km cm^{2b} GW^{-b} s^{-1} and $b = 1/3$.

(absorptivity, depth, size). The interesting feature leading to this result is that the laser damage can be analyzed considering the incubation fluence; the statistical analysis deduced from damage density measurements can be directly compared regarding this fluence for several experimental conditions.

III. ELEMENTS TO INTERPRET THE PROBABILISTIC BEHAVIOR REGARDING THE DETERMINISTIC ONE

A. Environment modification: Vacuum instead of air

Series of experiments have been conducted on fused silica samples exposed to two different environments: air and vacuum. The whole experimental conditions are detailed in Ref. 7. Precautions about hygrometry and cleanliness were taken in order to avoid any air breakdown during experiments in air environment. Damage densities (ρ) measurements were performed by means of the 1-on-1 procedure.[1] It appears clearly in Figure 3(a) that damage densities are lower (more than one order of magnitude) in air than in vacuum at a given fluence, or in the same way it is found that to reach a given damage density, fluences are much lower in vacuum than in air by a factor close to 0.66. Damage diameters (*dd*) of these sites are reported as function of total fluences (Figure 3(b)). It appears that there is no correlation between *dd* and F_{tot}. Following the procedures described in Sec. II, we have next matched the intensity profiles with the corresponding damage sites to evaluate incubation and expansion fluences: Figure 3(b) shows a good correspondence between *dd* and F_{exp} both in air and vacuum environments. Nonetheless *dd* increase with F_{exp} more rapidly in air than in vacuum. Indeed the parameters a et b of relation (3) are linked to the activation front speeds which are different in air and vacuum environments; a is equal to 9.3 km cm^{2b} GW^{-b} s^{-1} and 2.75 km cm^{2b} GW^{-b} s^{-1} where b is equal to 1/3 and 1/2, respectively, in air and vacuum.[7] These values are representative of the different physical processes involved in the formation of the ring pattern in both environments: the absence of air modifies significantly the plasma expansion phenomenon. The damage morphology originates from the simultaneous coupling of a laser supported ionization front propagating in air at 20 km/s with an ablation mechanism in silica leading to a larger damage site than in vacuum where the plasma is then confined at the vicinity of the surface, which is supposed to be "crawling" on the surface of the sample at 10 km/s. In air, the propagation of this ionization front is fast enough to outdo the mechanism occurring in vacuum and silica is no longer the support of the activation front (the surrounding air plays the role of a catalyst of the ring formation mechanisms).

From these measurements, the incubation fluences are deduced. Despite the scattering of the experimental data (Figure 3(c)) the mean value of incubation fluences is lower in vacuum than in air environments (35 and 50 J/cm^2, respectively, that is to say, a ratio close to 0.70 directly comparable to the ratio 0.66 found previously). Results from Figures 3(a) and 3(c) are complementary and consistent: the lower the incubation fluence, the higher the damage density at a given F_{tot}. Physical interpretations are in progress in order to explain such results: mechanical constraints could not be the same due to the stress difference which exists between the two faces of the optical components and/or precursor defects could be differently passivated because of the possible interaction of the atmospheric molecules with the optics surface.

B. ρ vs. F_{inc}: Simple approach based on the link between the damage site diameters and the precursor defect population

Figure 4 is a schematic illustration that describes a simple explanation of the results of Figure 3 by means of statistical and deterministic approaches. It will also help in the interpretation of the experimental results reported in Sec. IV. A schematic intensity profile is first considered based on a typical experimental MLM profile. Then, two different precursor populations are considered: a population of strongly reactive precursor defects (due to higher absorptivity or some other considerations), noted A in blue, and another population of weakly reactive precursor defects, noted B in red. These two populations are defined by a distribution of local defect damage thresholds.[5] Although these two populations are not well defined and known, most of the laser damage precursors at low fluence were found to be associated with fractures and scratches that occur during polishing and finishing.[15,16] At high fluences, Bude *et al.* have identified the precipitates as high fluence precursors due to chemical processing steps such as cleaning, etching, and rinsing for irradiation in the UV. It results in a variety of ionic species that can lead to optical damage.[17] These precursors are also good candidates in the case of IR irradiations. In vacuum environment, the correlation between more reactive absorbers and higher damage densities is theoretically studied

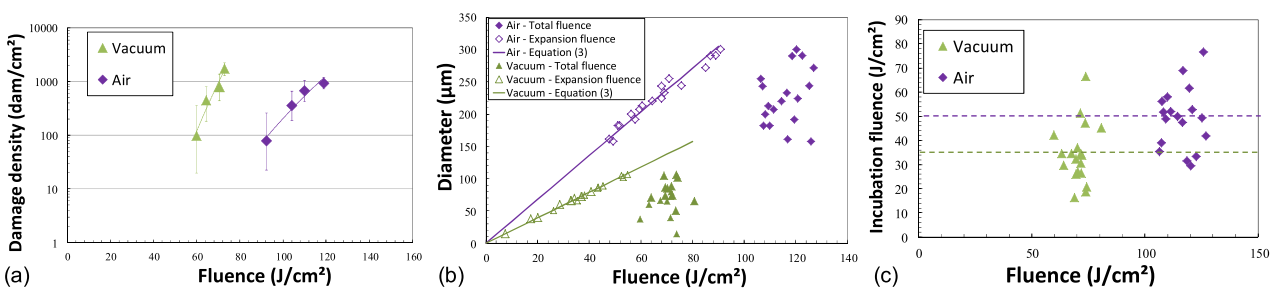

FIG. 3. Environment. Comparison between air and vacuum environments (violet and green, respectively). (a) Damage densities as a function of total fluence. (b) Damage diameter as a function of the total fluence (bold symbols) and the damage expansion fluence (empty symbols). (c) Incubation fluence as a function of the total fluence.

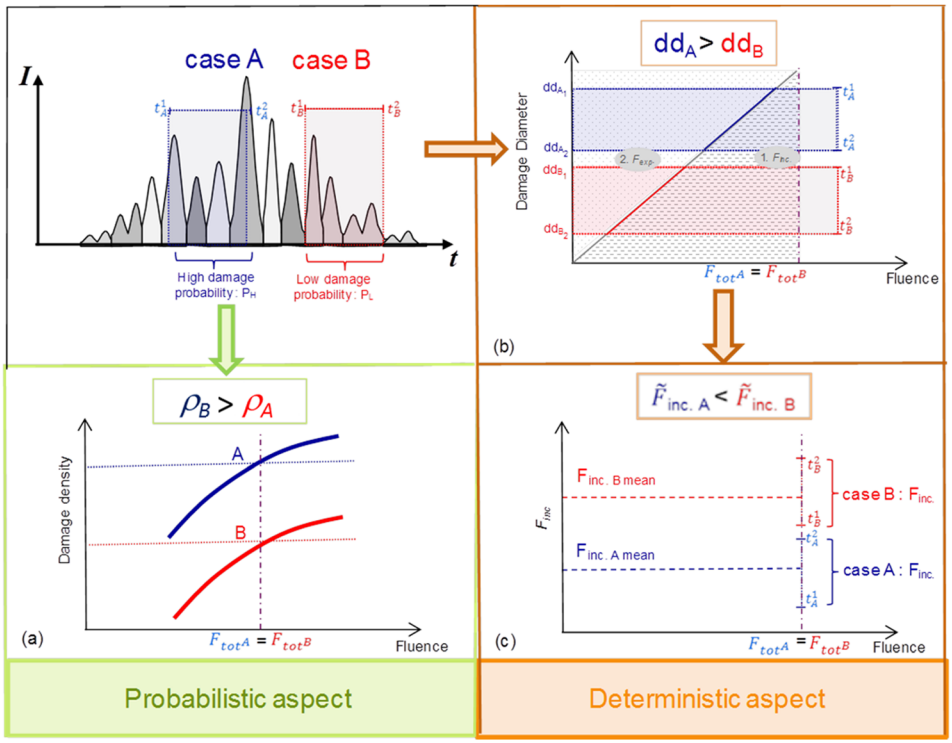

FIG. 4. Schematic illustration of the correspondence between (a) damage density, (b) damage diameter, and (c) incubation fluence induced by a schematic intensity profile of a MLM pulse. The hatched area (area 1. $F_{inc.}$) on (b) corresponds to the incubation fluence whereas the dotted area (area 2. $F_{exp.}$) corresponds to the expansion fluence. See text for the other details.

(subsurface fractures may be affected due to the stress; chemical modifications may also affect the defect absorptivity, etc.). We then consider the activation front starting times t_A and t_B for these two populations, respectively, A and B. The following statements are then proposed:

- Probabilistic approach, Fig. 4(a). At a given fluence, high damage density (ρ_A) is associated with the strongly reactive defects ensemble. On the contrary, a low damage density (ρ_B) is associated with the more weakly reactive precursors: then $\rho_A > \rho_B$.
- Deterministic approach, Fig. 4(b). The strongly reactive precursor defects are inclined to damage at the early stage of the pulse, which is schematically represented in the pulse by the activation front starting time interval ranging from t_A^1 to t_A^2. The expansion fluence associated with a damage site which activation front starts at t_A^1 is higher than the one of a damage site which activation front starts at t_A^2. This leads to a larger damage diameter: $dd_{A1} > dd_{A2}$ (blue dotted area).
- The less reactive precursor defects are inclined to damage at the end of the pulse, schematically stated by the interval from t_B^1 to t_B^2 in the pulse. The expansion fluence related to a damage site which activation front starts at t_B^1 is higher than the one of a damage site which activation front starts at t_B^2. Again, this leads to a larger damage diameter: $dd_{B1} > dd_{B2}$ (red dotted area).
- The more reactive precursor defects lead to large damage sites whereas the less reactive ones induce smaller damage sites (blue and red dotted areas, respectively): then $dd_A > dd_B$.
- Fig. 4(c): the incubation fluences related to the more reactive precursor defects ($F_{inc.A}$) are then lower than those associated with the less reactive ones ($F_{inc.B}$): then $F_{inc.A} < F_{inc.B}$.

In few words, let us retain the following adages: "the lower the incubation fluence, the higher the damage density (ρ)" and "the higher the expansion fluence, the larger the damage diameter (dd)." Several experimental results for different configurations are next analyzed following this approach in order to validate the methodology and to corroborate the statistical results (ρ).

IV. A POWERFUL TOOL TO INTERPRET LASER DAMAGE EXPERIMENTS (DISCRIMINATION BETWEEN PROBABILISTIC AND DETERMINISTIC BEHAVIORS BY MLM LASER PULSES)

A. Interpretation of damage results with the use of linear and circular polarizations

To compare damage densities of a same fused silica component for two states of beam polarization (linear and circular), the previous methodology was used. Figure 5(a) shows that the difference between damage densities is small (less than a decade, intervals of confidence[4] do not entirely overlap). Nonetheless this difference is much lower than the previous one reported in Fig. 3 concerning the effect of environment. To go further, we matched the MLM temporal profile with the ring pattern damage as the example shown in Fig. 6. Let us note first that this ring pattern is clearly formed: the central fractured area is quite small when compared to the one obtained with a linear polarization (Fig. 1). F_{exp} are then determined from several damage sites and again a linear relation links the dd with F_{exp} (Fig. 5(b)). There is no strong visual evidence that F_{inc} are different when comparing linear and circular polarizations but the analysis realized on numerous damage sites shows a slight difference: incubation fluences are in average close to 50 and 60 J/cm^2 for the linear and circular polarizations, respectively (a synthesis is reported in

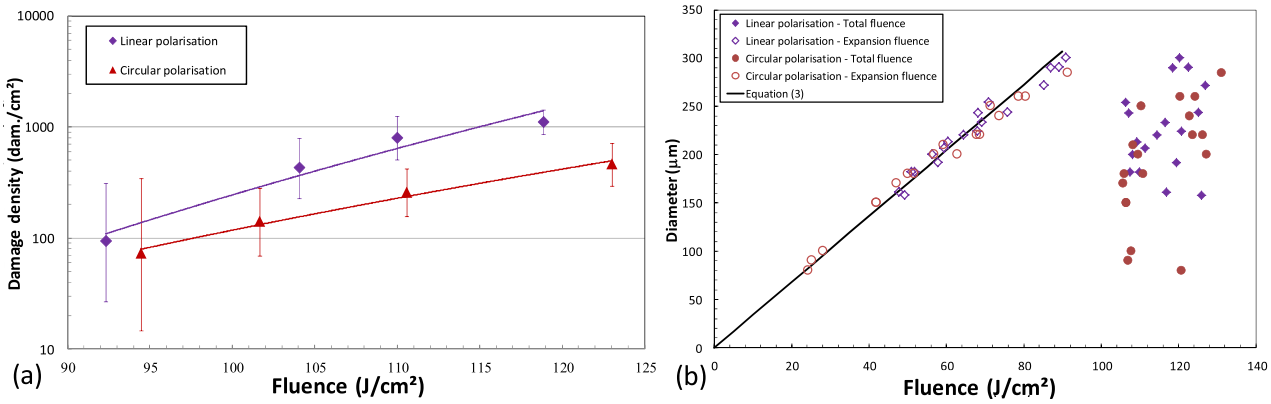

FIG. 5. Polarization. Comparison between circular and linear polarizations (brown and violet, respectively). (a) Damage densities as a function of total fluence. (b) Damage diameter as a function of the total fluence (bold symbols) and the damage expansion fluence (empty symbols).

Table I, Sec. V). Results from Figures 5(a) and 5(b) are consistent: the low difference obtained from damage density measurements is due to the slight difference between the incubation fluences of the two configurations. Indeed, it was shown that in the nonlinear regime, the probability for an electron to absorb photons is lower in the case of a circular polarization than in the case of a linear one.[18] Thus a circular polarization state might involve lower damage densities as it was found experimentally.

B. Interpretation of damage results obtained on different surface qualities: Polished or corrugated

This methodology was also used to compare two different optical surfaces: polished (superpolished by SESO Company) and corrugated (optical grating made of periodical pillars on the same superpolished component, this corrugated optics was described and previously used in Ref. 7). It was observed that the formation of a ring pattern still takes place when irradiations are performed in air environment on this corrugated component. It was next shown that the ring appearance speed on a damage site follows the same power law whatever the optical surfaces and then that the expansion phase leading to the formation of the ring pattern does not depend on the sample surface state. As a consequence damage densities measured on these components (Fig. 7(a)) can be directly compared with damage diameters (*dd*) of the related damaged sites (Fig. 7(b)). From these results, once again *dd* follows a linear relation versus F_{exp} and not versus F_{tot} for both optical surfaces. Next the incubation fluence is lower for the corrugated surface than for the polished surface (30 and 50 J/cm^2, respectively) which is finally consistent with a much higher damage density for the corrugated surface than for the polished surface (more than one order of magnitude at a given fluence (Fig. 7(a)): the lower the incubation fluence, the higher the damage density. This difference is likely due to the electric field enhancement with the corrugation,[19] considering that damage precursors are the same for both samples.

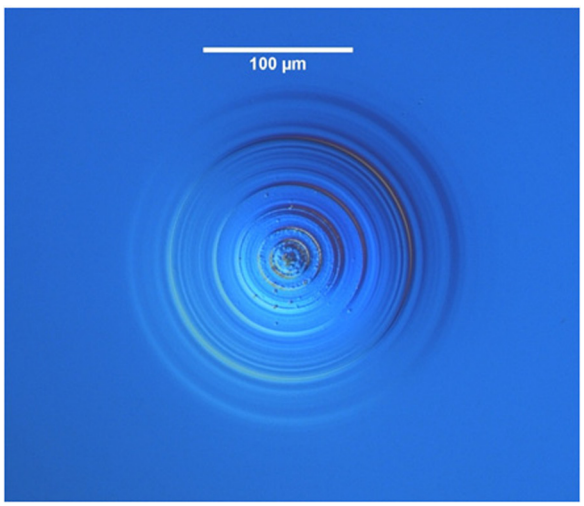

FIG. 6. Nomarski interference contrast image of a damage site initiated in air environment by a MLM circular pulse.

C. Single longitudinal mode (SLM) regime

It was also possible to follow the same methodology for single longitudinal mode (SLM) pulses and then to make a comparison between SLM and MLM laser damage tests. Concerning damage densities, at a given fluence (110 J/cm^2, for example), the damage density is a decade lower in SLM regime than in MLM one (Figure 8(a)). SLM pulses are characterized by a smooth and regular Gaussian temporal profile (Fig. 9(c)), stable shot to shot (an injection seeder in the cavity laser assures the mode to be stable[20] without an overshoot[21]). SLM damage sites are characterized by a damaged central area surrounded by a smooth funnel-shaped surface ablation (Fig. 9(b)). The optical profilometer measurement

TABLE I. Mean incubation fluences $\tilde{F}_{inc}$ corresponding to different experimental configurations for optical components submitted to the same polishing process. The reported configurations are as follows: Laser mode—Environment—Laser polarization. The last column indicates the figure corresponding to the data.

Configuration	$\tilde{F}_{inc}$ (J/cm^2)	Figure
1/SLM—Air—Linear polarization	70	9
2/MLM—Air—Linear polarization	50	3 and 9
3/MLM—Air—Circular polarization	60	5
4/SLM—Vacuum—Linear polarization	45	Not reported
5/MLM—Vacuum—Linear polarization	35	3

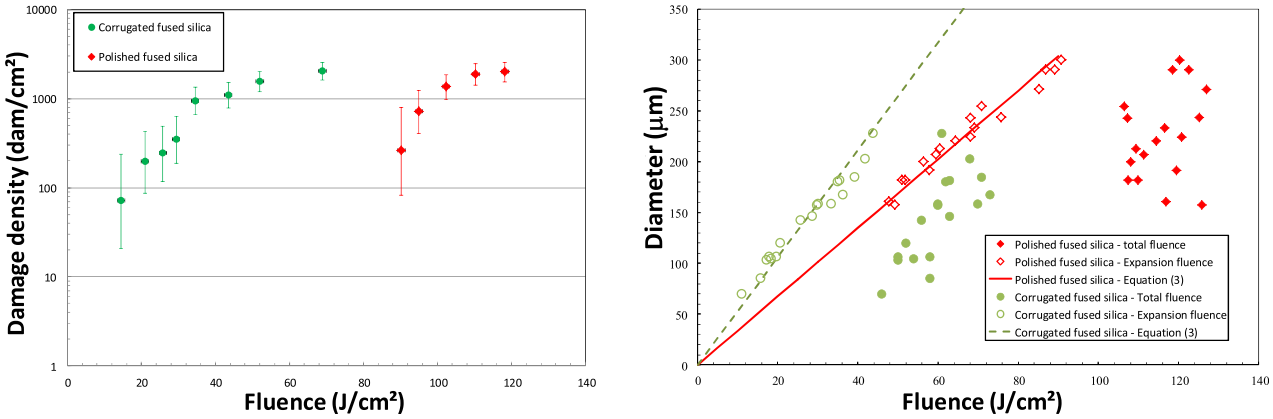

FIG. 7. Surface. Comparison between corrugated fused silica and polished fused silica (green and red, respectively). (a) Damage densities as a function of total fluence. (b) Damage diameters as a function of the total fluence (bold symbols) and the damage expansion fluence (empty symbols).

shows that this modification corresponds to a smooth decrease (≈700 nm) towards a central fractured area (Fig. 9(a)). This smooth decrease is well correlated to the smooth corresponding temporal profile after t_0. The determination of F_{inc} and F_{exp} in case of SLM regime is based on the same principle: the outer diameter of the damage site is matched with the end-foot of the temporal profile (fixed for all sites at 5% of I_{max}, dashed line labelled 2 in Fig. 9) allowing the determination of t_0. Again, the two damage formation phases are distinguished and it was found that, in most cases, t_0 is at the top of the SLM temporal profile meaning that incubation fluence and expansion fluence are quite similar. From Equation (3) and the measure of the damage diameter, the expansion fluence is then precisely determined (the parameters a and b being those determined from the experiments realized in the MLM configuration). It appears in Figure 8(b) again, a linear relation between dd and F_{exp}, and not with F_{tot} whatever the laser mode configurations are (MLM and SLM). The two slopes (red and blue lines) obtained with Equation (3) are slightly different. Indeed, here the experimental conditions are the same (air environment), it means that a and b parameters from relation (3) are the same. The different slopes are then only due to the different F_{tot} during experiments. From the results reported in Figure 8(b), it was found that F_{inc} is lower in the MLM regime than in the SLM one (about 50 J/cm^2 and 70 J/cm^2, respectively): once again, the lower the F_{inc}, the higher the damage density. This behavior was explained in Ref. 22 by the enhancement of the three-photon absorption due to the intensity spikes related to MLM pulses, these pulses are more inclined to give rise to multi-photon absorption than SLM ones.

V. SUMMARY AND CONCLUSION

To go further on the interpretation of examples presented in Section IV, the incubation fluence was quantified for each experiment. To this end, F_{inc} has been deduced for each experimental damage site calculating the difference between F_{tot} and F_{exp} as reported in Figure 2. It permits to obtain numerous data as those reported in Figure 3(c). These data are scattered due to damage precursors distribution (in nature and size). However a mean value of incubation fluence $\tilde{F}$ is extracted. This mean incubation fluence highlights the statistical nature of the nanosecond damage governed by the defect ensemble damage threshold distribution. The linear relation between damage diameter and expansion fluence shows a deterministic aspect of the nanosecond damage. Table I reports the synthesis of these values obtained for the

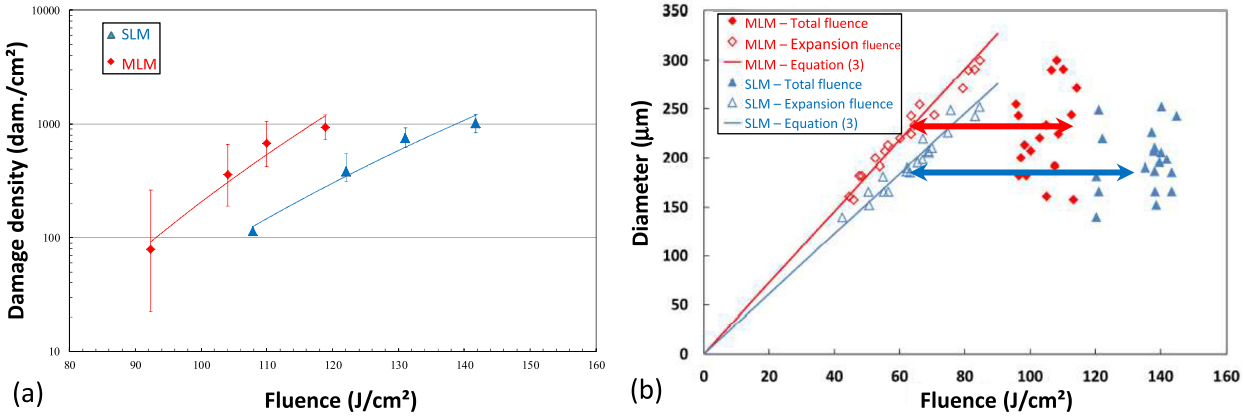

FIG. 8. Comparison between MLM and SLM configurations (red and blue, respectively). (a) Damage densities as a function of total fluence. (b) Damage diameter as a function of the total fluence (bold symbols) and the damage expansion fluence (empty symbols). The red and blue arrows report the mean incubation fluence for a given laser configuration.

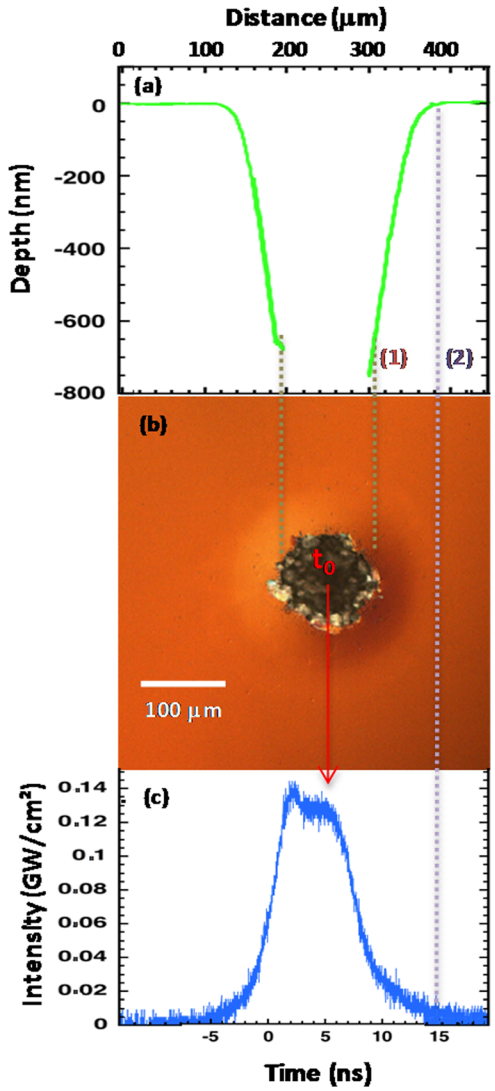

FIG. 9. Characterization of a damage site initiated by a single longitudinal mode pulse. (a) Optical profilometer analysis. (b) Nomarski interference contract microscope picture and (c) temporal profile.

different experimental configurations on components with the same polishing process. It allows one to compare two different configurations and thus the effect of each laser parameter:

- Comparing configurations 1/ and 2/ (and 4/ with 5/), it appears that $\tilde{F}_{inc}$ is lower for MLM pulses than for SLM ones; it is consistent with the fact that ρ in MLM configuration is higher than in the SLM one. These two results indicate that the MLM pulses are more inclined to trigger the damage than the SLM ones. This behavior is attributed to the overshoot in the temporal profile leading to high intensities and thus multi-photon absorption with MLM pulses.
- Comparing configurations 2/ and 3/, it appears that $\tilde{F}_{inc}$ is lower for the linear polarization than for the circular one; it is consistent with the fact that ρ for the linear polarization is higher than for the circular one. These two results indicate that the linear polarization is more inclined to trigger the damage than the circular one. This fact is likely due to the higher probability of the electron to absorb several photons in case of a linear polarization.
- Comparing configurations 1/ and 4/ (and 2/ with 5/), it appears that $\tilde{F}_{inc}$ is lower for experiments realized in vacuum environment than in air environment; it is consistent with the fact that ρ in vacuum environment is higher than in air environment. These two results indicate that vacuum environment (as described in Ref. 7) is more inclined to trigger the damage than the air environment: different mechanical constraints due to stress could lead to this result, as well as possible interactions between atmospheric components and optics surface.

The damage diameters obtained and measured during these 1064 nm ns laser irradiations are much larger (in the range 50–200 μm) than the ones reported in Ref. 23 (in the range 2–20 μm). Simulations and experiments by Carr *et al.* at 355 nm (3.5 eV) on fused silica have shown that after damage initiates (corresponding to the incubation phase), energy is deposited in a laser-supported absorption front which grows with the pulse length away from the initial site of precursor absorption (corresponding to the expansion fluence).[23] The longer pulses result then in larger cores. Nonetheless core diameters are smaller than 20 μm. This difference is likely due to the fact that at 355 nm, for laser intensities around 10 GW/cm^2, the maximum electron energy calculated by Chambonneau *et al.* is around 6 eV, making impossible the starting of an electron avalanche.[11] It means that the ionization front propagating in air is not possible, and a detonation-like wave is not involved at 355 nm as at 1064 ns leading *in fine* to much smaller damage sites.

To conclude, MLM pulses provide a powerful tool that allows one to investigate the chronology of the physical processes involved in LID for different configurations. There is a strong relation between the expansion phase subsequent to incubation and the final damage diameters. Actually, the estimation of the expansion fluence from the final diameter is only possible, thanks to the knowledge of the activation front speeds.[6,7] By means of the incubation fluence determination (deduced from the precise determination of the expansion fluence), this methodology allows the interpretation of statistical results like damage density measurements. It is really efficient too in case of a very fine difference like the effect of laser polarization (linear vs. circular, Sec. IV A). Furthermore, this methodology has been applied with success to SLM pulses (Sec. IV C) despite the lack of the ring pattern (in that case the silica surface is ablated in a regular way and no ring appears), the physical processes and the damage chronology (incubation phase followed by expansion phase) being the same.

[1]ISO Standard Nos. 21254-1–21254-4 (2011).
[2]J. Y. Natoli, L. Gallais, H. Akhouayri, and C. Amra, "Laser-induced damage of materials in bulk, thin-film, and liquid forms," Appl. Opt. **41**, 3156 (2002).
[3]L. Lamaignère, T. Donval, M. Loiseau, J. C. Poncetta, G. Raze, C. Meslin, B. Bertussi, and H. Bercegol, "Accurate measurements of laser-induced bulk damage density," Meas. Sci. Technol. **20**, 095701 (2009).
[4]L. Lamaignère, S. Bouillet, R. Courchinoux, T. Donval, M. Josse, J. C. Poncetta, and H. Bercegol, "An accurate, repeatable, and well characterized measurement of laser damage density of optical materials," Rev. Sci. Instrum. **78**, 103105 (2007).

[5]G. Bataviciute, M. Sciuka, and A. Melninkaitis, "Direct comparison of defect ensembles extracted from damage probability and raster scan measurements," J. Appl. Phys. **118**, 105306 (2015).
[6]M. Chambonneau, P. Grua, J.-L. Rullier, J.-Y. Natoli, and L. Lamaignère, "Parametric study of the damage ring pattern in fused silica induced by multiple longitudinal modes laser pulses," J. Appl. Phys. **117**, 103101 (2015).
[7]R. Diaz, M. Chambonneau, P. Grua, J. L. Rullier, J. Y. Natoli, and L. Lamaignère, "Influence of vacuum on nanosecond laser-induced surface damage morphology in fused silica at 1064 nm," Appl. Surf. Sci. **362**, 290 (2016).
[8]S. Papernov and A. W. Schmid, "Two mechanisms of crater formation in ultraviolet-pulsed-laser irradiated SiO_2 thin films with artificial defects," J. Appl. Phys. **97**, 114906 (2005).
[9]J. O. Porteus and C. Seitel, "Absolute onset of optical surface damage using distributed defect ensembles," Appl. Opt. **23**, 3796 (1984).
[10]S. C. Jones, P. Braunlich, R. T. Casper, X.-A. Shen, and P. Kelly, "Recent progress on laser-induced modifications and intrinsic bulk damage of wide-gap optical materials," Opt. Eng. **28**, 281039 (1989).
[11]M. Chambonneau, R. Diaz, P. Grua, J.-L. Rullier, G. Duchateau, J.-Y. Natoli, and L. Lamaignère, "Origin of the damage ring pattern in fused silica induced by multiple longitudinal modes laser pulses," Appl. Phys. Lett. **104**, 021121 (2014).
[12]H. Bercegol and P. Grua, "Fracture related initiation and growth of surface laser damage in fused silica," Proc. SPIE **7132**, 71321B (2008).
[13]N. Bloembergen, "Laser-induced electric breakdown in solids," IEEE J. Quantum Electron. **10**, 375 (1974).
[14]P. Grua, D. Hébert, L. Lamaignère, and J.-L. Rullier, "Role of suprathermal electrons during nanosecond laser energy deposit in fused silica," Appl. Phys. Lett. **105**, 081902 (2014).
[15]T. A. Laurence, J. D. Bude, S. Ly, N. Shen, and M. D. Feit, "Extracting the distribution of laser damage precursors on fused silica surfaces for 351 nm, 3 ns laser pulses at high fluences (20–150 J/cm^2)," Opt. Express **20**, 11561 (2012).
[16]T. A. Laurence, J. D. Bude, N. Shen, T. Feldman, P. E. Miller, W. A. Steele, and T. Suratwala, "Metallic-like photoluminescence and absorption in fused silica surface flaws," Appl. Phys. Lett. **94**, 151114 (2009).
[17]J. Bude, P. Miller, S. Baxamusa, N. Shen, T. Laurence, W. Steele, T. Suratwala, L. Wong, W. Carr, D. Cross, and M. Monticelli, "High fluence laser damage precursors and their mitigation in fused silica," Opt. Express **22**, 5839 (2014).
[18]V. V. Temnov, K. Sokolowski-Tinten, P. Zhou, A. El-Khamhawy, and D von der Linde, "Multiphoton ionization in dielectrics: Comparison of circular and linear polarization," Phys. Rev. Lett. **97**, 237403 (2006).
[19]N. Bonod and J. Néauport, "Diffraction gratings: From principles to applications in high-intensity lasers," Adv. Opt. Photonics **8**, 156 (2016).
[20]Y. K. Park, G. Giuliani, and R. L. Byer, "Stable single-axial-mode operation of an unstable-resonator Nd:YAG oscillator by injection locking," Opt. Lett. **5**, 96 (1980).
[21]R. Diaz, R. Courchinoux, J. Luce, C. Rouyer, J. L. Rullier, J. Y. Natoli, and L. Lamaignère, "Experimental evidence of temporal and spatial incoherencies of Q-switched Nd:YAG nanosecond laser pulses," Appl. Phys. B **121**, 439 (2015).
[22]R. Diaz, M. Chambonneau, R. Courchinoux, P. Grua, J. Luce, J.-L. Rullier, J.-Y. Natoli, and L. Lamaignère, "Influence of longitudinal mode beating on laser-induced damage in fused silica," Opt. Lett. **39**, 674 (2014).
[23]C. W. Carr, J. D. Bude, and P. DeMange, "Laser-supported solid-state absorption fronts in silica," Phys. Rev. B **82**, 184304 (2010).